Consistency between ARPES and STM measurements on SmB_6

Christian E. Matt,[1] Harris Pirie,[1] Anjan Soumyanarayanan,[1,*] Yang He,[1] Michael M. Yee,[1] Pengcheng Chen,[1] Yu Liu,[1] Daniel T. Larson,[1] Wendel S. Paz,[2,3] J. J. Palacios,[4,5] M. H. Hamidian,[1] and Jennifer E. Hoffman[1,†]

[1]*Department of Physics, Harvard University, Cambridge, Massachusetts 02138, USA*

[2]*Departamento de Física, Universidade Federal do Espírito Santo (UFES), Av. Fernando Ferrari, 514, 29075-910, Vitória, ES, Brazil*

[3]*Instituto de Física, Universidade Federal do Rio de Janeiro, Caixa Postal 68528, Rio de Janeiro, RJ 21941-972, Brazil*

[4]*Departamento de Física de la Materia Condensada, Condensed Matter Physics Center (IFIMAC) and Instituto Nicolás Cabrera (INC), Universidad Autónoma de Madrid, Cantoblanco, 28049 Madrid, Spain*

[5]*Department of Physics, The University of Texas at Austin, Austin, Texas 78712, USA*

(Received 10 July 2019; revised manuscript received 10 December 2019; accepted 16 December 2019; published 28 February 2020)

The Kondo insulator SmB_6 has emerged as a primary candidate for exotic quantum phases, due to the predicted formation of strongly correlated, low-velocity topological surface states and corresponding high Fermi-level density of states. However, measurements of the surface-state velocity in SmB_6 differ by orders of magnitude, depending on the experimental technique used. Here we reconcile two techniques, scanning tunneling microscopy (STM) and angle-resolved photoemission spectroscopy (ARPES), by accounting for surface band bending on polar terminations. Using spatially resolved scanning tunneling spectroscopy, we measure a band shift of ∼20 meV between full-Sm and half-Sm terminations, in qualitative agreement with our density-functional theory calculations of the surface charge density. Furthermore, we reproduce the apparent high-velocity surface states reported by ARPES by simulating their observed spectral function as an equal-weight average over the two band-shifted domains that we image by STM. Our results highlight the necessity of local measurements to address inhomogeneously terminated surfaces or fabrication techniques to achieve uniform termination for meaningful large-area surface measurements of polar crystals such as SmB_6.

DOI: 10.1103/PhysRevB.101.085142

I. INTRODUCTION

In a Kondo insulator (KI), strong interactions between localized f electrons renormalize their spectral weight toward the chemical potential. Below a characteristic temperature T^*, conduction electrons begin to scatter from these renormalized f states, opening a hybridization gap at the Fermi level. In a subset of KIs called topological KIs, this gap can encode a nontrivial bulk topological invariant, leading to the appearance of protected surface states [1,2]. In the KI SmB_6, the onset of the hybridization gap leads to a resistivity upturn below ∼50 K [3–5]. Yet, rather than diverging, the resistivity saturates below 5 K, indicating the emergence of an additional conduction channel [6,7]. This conduction channel has been attributed to topological surface states by several theoretical studies, which span complementary approaches including renormalized band theory and tight-binding Hamiltonians matched to LDA (+Gutzwiller) calculations [8–10]. These calculations predict the existence of three surface Dirac cones with heavy quasiparticles, of predominantly f character, as shown schematically in Fig. 1. Such low-velocity Dirac fermions would provide a high density of states at the Fermi level, increasing their susceptibility to exotic orders and their potential utility [10–13]. However, the empirical identification of the additional conduction channel [6,7] with the predicted topological surface states [8–10] has remained controversial due to apparent contradictions between different experimental techniques.

Experimentally, angle-resolved photoemission spectroscopy (ARPES) and scanning tunneling microscopy (STM) have each identified key features of the topological states in SmB_6, but with quantitative and qualitative differences. At low temperatures, ARPES studies reported a hybridization gap that hosts linearly dispersing surface states [14–18] with a nontrivial spin texture [19,20]. However, the apparent velocity of these states is an order of magnitude higher than theoretically predicted (see Table I). Meanwhile, the hallmark of a topological surface state—its Dirac point—has not been clearly resolved in any ARPES experiment to date [16], leading to the suggestion that it has been pushed into the valence band by a strong surface potential [23], or by the breakdown of the Kondo effect at the surface [24]. On the other hand, milliKelvin scanning tunneling spectroscopy (STS) studies identified several strong resonances within the hybridization gap, consistent with low-velocity surface states [25,26]. Additionally, momentum-resolved STM directly imaged linearly dispersing low-velocity surface states that converge to a Dirac point within the gap [21], consistent with theoretical predictions [9].

The apparent inconsistencies between STM and ARPES arise from the different experimental length scales for each technique. STM typically images hundred-nanometer regions with picometer spatial resolution. On SmB_6, STM universally

*Present address: Institute of Materials Research and Engineering, Agency for Science, Technology and Research, Singapore.

†jhoffman@physics.harvard.edu

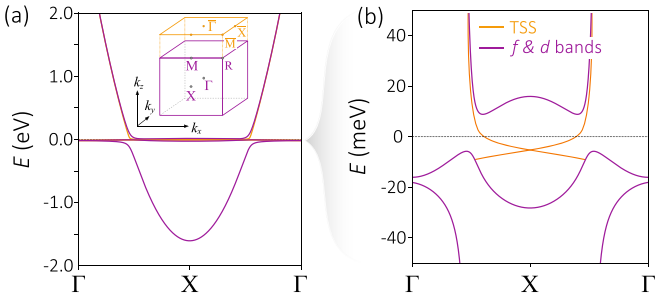

FIG. 1. (a) Schematic of the SmB_6 band structure, showing two heavy f bands hybridizing with a light d band (all purple), and topological surface states (TSS, orange) that have a low velocity. Inset of (a): Bulk and surface Brillouin zone of SmB_6. (b) Zoom-in of band structure at the Fermi level.

observes surface domains with sizes on the order of tens of nanometers [21,25–29], consistent with its polar structure and the lack of a natural cleavage plane. Yet the typical ARPES spot size is on the order of tens of microns [30] and consequently averages over thousands of SmB_6 surface domains. This averaging poses a problem if the various domains exhibit polarity-driven band bending, as ARPES spectra will contain a superposition of spectral features, shifted in energy with respect to one another.

Here we use STM spectroscopy to guide a simulation of the spectral functions on polar Sm 1×1 and nonpolar Sm 2×1 terminations, using the energy and momentum broadening of typical ARPES experiments. For a range of realistic experimental parameters, our *simulated* ARPES spectra show topological surface states with an artificially enhanced Fermi velocity and a buried Dirac point, similar to published *experimental* ARPES results. Our findings provide the long-sought, fully consistent explanation for the apparent discrepancy between the band structure measured by ARPES and STM. They further confirm the consistency between STM and theoretical predictions of low-velocity surface states with an in-gap Dirac point and high density of states at the Fermi level.

II. METHODS

A. Scanning tunneling microscopy/spectroscopy

We performed STM experiments on single crystals of SmB_6 grown using the Al-flux method [31,32]. We cleaved the crystals in cryogenic ultrahigh vacuum at ∼30 K before inserting them into the STM head. We prepared PtIr STM tips by *ex situ* mechanical sharpening then *in situ* field emission on Au foil.

B. Calculations

We performed calculations in the framework of density-functional theory (DFT), as implemented in the QUANTUM ESPRESSO package [33]. We calculated the exchange-correlation functional using the generalized gradient approximation of Perdew-Burke-Ernzerhof [34]. The electron-ion interactions are described by ultrasoft pseudopotentials with valence electron configurations of $2s^2 2p^1$ for B atoms and $5s^2 4d^{10} 5p^6 6s^2 4f^6$ for Sm atoms. The energy cutoff for the plane-wave basis is 120 Ry with a charge-density cutoff of 500 Ry. We used a Monkhorst-Pack [35] scheme with a $12 \times 12 \times 1$ k mesh for the Brillouin zone integration for the supercell with one unit cell (1×1 Sm) and $6 \times 12 \times 1$ k mesh for the supercell with two unit cells (2×1 Sm). In all calculations, the lattice parameter was fixed at the experimental value $a_0 = 4.13$ Å, with slab thickness 20.65 Å and vacuum thickness 15 Å to minimize interactions between the periodic images. We did not consider spin polarization or spin-orbit coupling since our focus is on the electrostatics of the material.

III. RESULTS

A. Surface characterization

Due to its lack of a natural cleavage plane, an abundance of distinct surface terminations have been observed by STM on SmB_6 [36]. Across a dozen STM experiments, the largest reported domain of an ordered surface on pristine SmB_6 (<1% dopants) is only 60 nm [21,25–29,36–38]. Two commonly observed surfaces are the 1×1 square lattice [Fig. 2(a)] and the 2×1 rows that arise when half of the Sm atoms are removed during cleaving [Figs. 2(b) and 2(c)] [36,39]. The 2×1 surface has also been observed by low-energy electron diffraction [40] and ARPES, where it manifests as Umklapp scattering [15,41]. We confirmed the identity of the 2×1 surface using lightly Fe-doped samples where Fe is known to substitute for Sm [42]; we observed individual Fe-atom signatures centered on the rows of Sm atoms in Fig. 2(c). We confirmed the identity of the 1×1 lattice presented in Fig. 2(a) as a full Sm layer due to the direction of its band bending compared to the 2×1 surface, as shown in Figs. 2(d) and 2(e) and discussed in more detail below.

The relative prevalence of each surface can be understood from its formation energy [Figs. 2(f)–2(h)]. Although most STM reports have focused on the 1×1 surface [25–28], our

TABLE I. Comparison of SmB_6 surface-state properties predicted by theory and measured by STM, ARPES, and quantum oscillations. We tabulate values for the Fermi velocity v, Dirac-point energy E_D, and surface Fermi wave vector k_F, at both the $\bar{X}$ and $\bar{\Gamma}$ points of the surface Brillouin zone.

	Theory [9]	STM [21]	ARPES [18]	Quantum oscillation [22]
$\hbar v_{\bar{X}}$ (meV Å)	7.6 ± 0.3	16 ± 2	240 ± 20	1900 ± 300
$E_{D_{\bar{X}}}$ (meV)	-5.4 ± 0.1	1 ± 1	-65 ± 4	-57 ± 9
$(k_{F_{\bar{X}}} - \bar{X})(\pi/a_0)$	0.44 ± 0.06	0.19 ± 0.02	0.51 ± 0.03 ($\Gamma - X - \Gamma$)	0.039 ± 0.003
$\hbar v_{\bar{\Gamma}}$ (meV Å)	90 ± 9	50 ± 2	220 ± 20	4300 ± 100
$E_{D_{\bar{\Gamma}}}$ (meV)	-9 ± 2	-7 ± 1	-23 ± 3	-460 ± 20
$k_{F_{\bar{\Gamma}}}(\pi/a_0)$	0.07 ± 0.01	0.14 ± 0.02	0.15 ± 0.03	0.142 ± 0.001

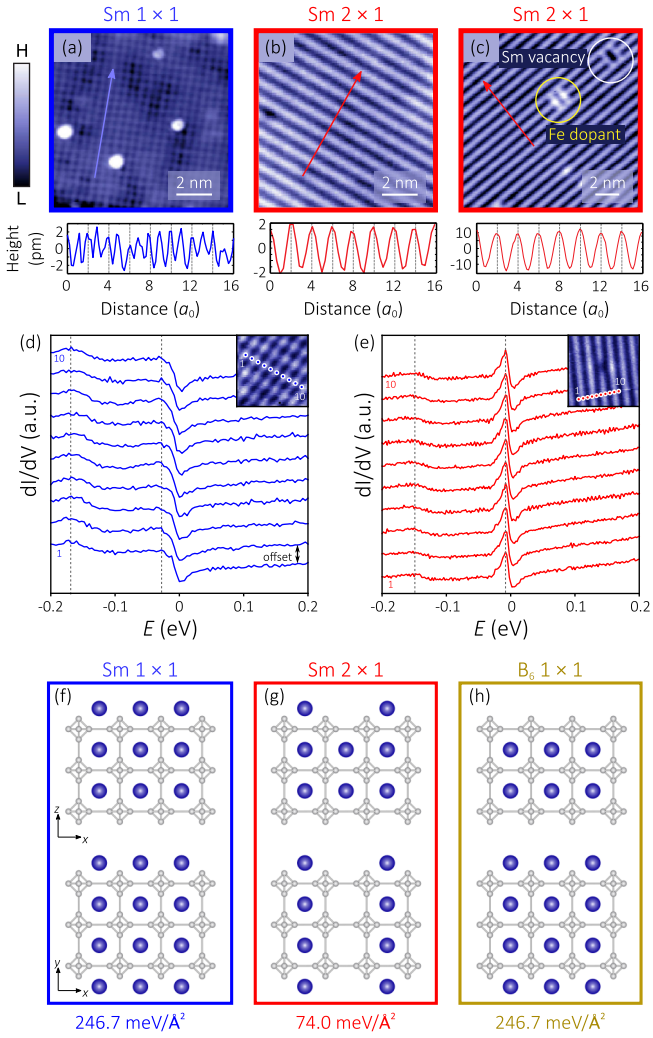

FIG. 2. STM topography of the (a) Sm 1 × 1 termination and the Sm 2 × 1 termination of (b) pristine SmB_6 and (c) Fe-doped SmB_6 [21]. Acquisition parameters are (a) $V_s = 200\,\text{mV}$, $R_J = 10\,\text{G}\Omega$ (b) $V_s = 100\,\text{mV}$, $R_J = 5\,\text{G}\Omega$, and (c) $V_s = 100\,\text{mV}$, $R_J = 0.5\,\text{G}\Omega$. (d), (e) Spatially homogeneous dI/dV spectra on the Sm 1 × 1 and Sm 2 × 1 surface. Each curve is offset for clarity. The location is indicated in the inset of each panel. The inset in (d) shows an area of 2.5 × 2.5 nm² and (e) an area of 5.1 × 5.1 nm². Acquisition parameters are (d) $T = 9.5\,\text{K}$, $V_s = -200\,\text{mV}$, $R_J = 2\,\text{G}\Omega$, bias excitation amplitude $V_{\text{rms}} = 2.82\,\text{mV}$, and (e) $T = 6.5\,\text{K}$, $V_s = 200\,\text{mV}$, $R_J = 1\,\text{G}\Omega$, $V_{\text{rms}} = 1.41\,\text{mV}$. (f)–(h) Side-view (upper) and top-view (lower) of different surface terminations and their corresponding formation energies, calculated by DFT.

more frequent observation of the 2 × 1 surface is consistent with its lower formation energy as calculated by DFT. In general, a more balanced charge distribution on either side of the cleave, as drawn in Fig. 2(g), is intuitively expected to lower the surface formation energy.

B. Termination-dependent band bending

In general, the surface termination can cause a redistribution of charge that affects the local electronic structure, an effect well studied in conventional semiconductors [43]. In

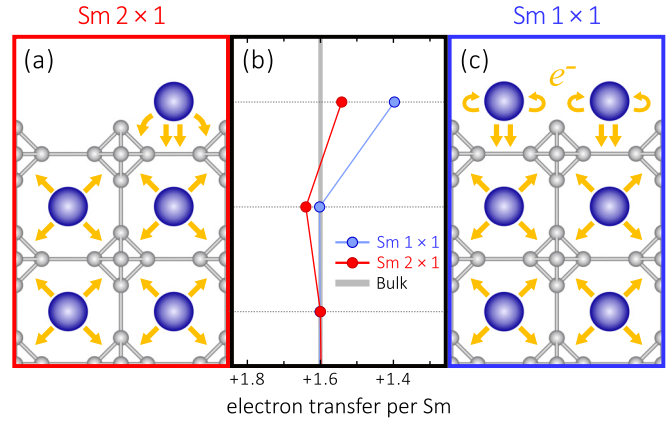

FIG. 3. DFT-calculated electron transfer from Sm atoms to B_6 clusters for the 2 × 1 surface (a) and the 1 × 1 surface (c). Fewer electrons are drawn from each Sm atom on the 1 × 1 surface as compared to the 2 × 1 surface.

bulk SmB_6, Sm atoms donate equal amounts of charge to the B_6 octahedra above and below them. However, on the 1 × 1 surface the Sm atoms are undercoordinated; the B layer beneath the topmost Sm layer cannot accept all of the excess electrons, so they accumulate on the surface. This charge accumulation is qualitatively captured in our calculations of the electron transfer, which use Bader analysis to partition the DFT charge density [Fig. 3].

The increased electron density near the 1 × 1 surface leads to reduced surface charge transfer, shown as a blue line in Fig. 3(b), greater filling of the Sm orbitals, and to a slight downward bending of the surface bands. On the other hand, Sm atoms at the 2 × 1 surface can donate a greater fraction of their electrons to the B layer below, because there are only half as many Sm atoms at the surface as in the bulk. Correspondingly, we found only a minor deviation in the calculated charge transfer at the 2 × 1 surface, shown as a red line in Fig. 3(b). Although our Bader charge analysis quantitatively departs from the experimental Sm valence of around +2.5 [44], it provides a qualitative understanding of the charge transfer on the SmB_6 surface.

To experimentally determine the accumulation of surface charge, we measured local differential conductance, $dI/dV(\mathbf{r}, E)$, where I is the tunneling current and V is the bias applied to the sample with respect to the tip. On a typical ordered domain, there are three pronounced spectral features: a peak around −150 meV, a peak just below E_F, and a shoulder around 40 meV, as shown in Fig. 4(a). The two filled-state peaks predominantly reflect contributions from the Sm $4f$ states, as determined by previous STM and ARPES measurements, and by dynamical mean-field theory calculations [21,26,29,45]. Although the peak energies are homogeneous within each ordered domain [see Figs. 2(d) and 2(e)], we found that the peaks are shifted downward on the 1 × 1 surface by about 20 meV compared to the 2 × 1 surface.

C. Spectral function simulation

ARPES spectra can be broadened by local band bending if the spot size encompasses multiple surface domains of

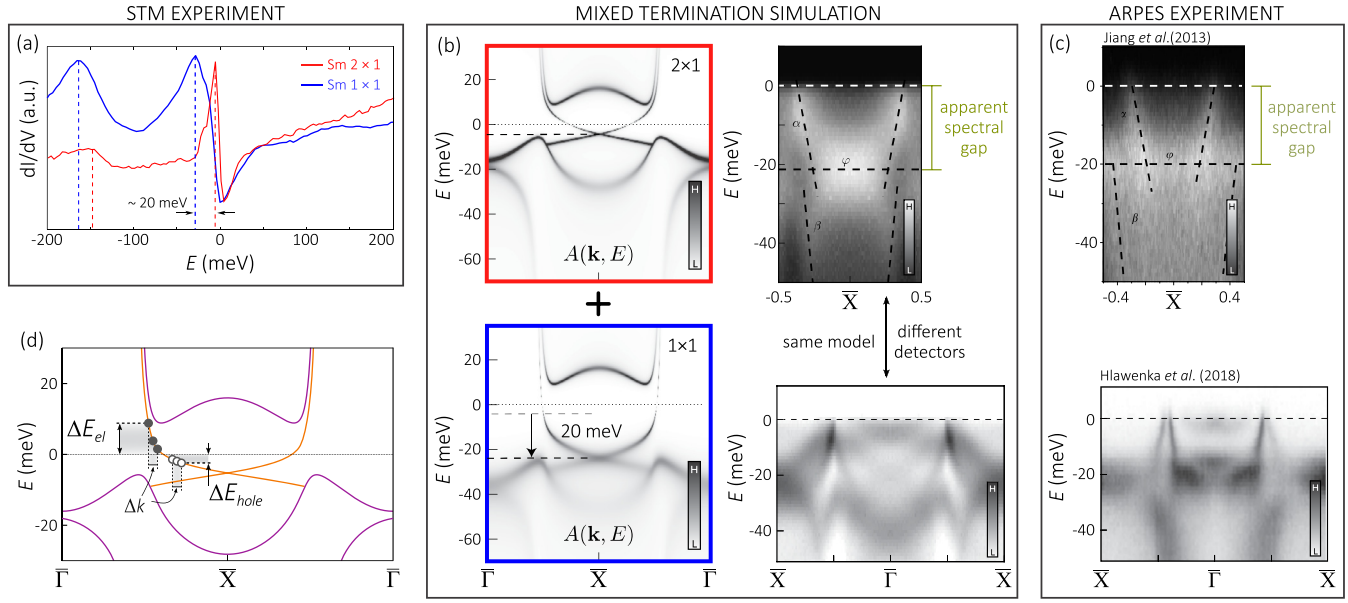

FIG. 4. (a) Measured dI/dV on two different surfaces of SmB_6. Acquisition parameters are (blue curve) $T = 9$ K, $V_s = -250$ mV, $R_J = 2$ GΩ, bias excitation amplitude $V_{rms} = 2.8$ mV, and (red curve) $T = 8$ K, $V_s = 200$ mV, $R_J = 1$ GΩ, $V_{rms} = 1.4$ mV. (b) Starting with the electronic structure derived by STM on the nonpolar 2×1 surface (red) [21], we inferred the electronic structure on the 1×1 polar termination by rigidly shifting the occupied states down by 20 meV (blue), based on our local STS measurements. The average of the simulated spectral functions from the 2×1 and 1×1 surfaces imitates the result of a spatially averaging measurement such as ARPES. We convoluted the averaged spectral function with a Gaussian kernel to account for finite temperature, energy, and momentum resolution. The following realistic experimental parameters have been used to simulate the spectra along the $\overline{M} - \overline{X} - \overline{M}$ and $\overline{X} - \overline{\Gamma} - \overline{X}$ directions. Upper panel: $T = 12$ K, $\Delta E = 10$ meV, $\Delta k = 0.04$ Å^{-1} (as reported in Ref. [18]); lower panel: $T = 1$ K, $\Delta E = 3$ meV, $\Delta k = 0.01$ Å^{-1} (as reported in Ref. [41]). Furthermore, we included band folding as described in Ref. [41] for the simulation presented in the lower panel. Despite the low-velocity Dirac fermions we started with, both simulations give the appearance of high-velocity states at the Fermi level that reproduce the ARPES experimental data presented in Refs. [18,41]. (c) Two different ARPES intensity maps are reproduced from Refs. [18,41] for direct comparison with our mixed-termination simulations in panel (b). (d) Adding electrons increases the Fermi level by a large amount due to the high velocity of the surface states above the chemical potential, whereas removing electrons decreases the Fermi level by only a small amount given the low surface state velocity below the chemical potential.

different polarities. We investigated this possibility in SmB_6 by deriving a spectral function for each termination from our STM measurements [21]. In accordance with our data, our simulation includes low-velocity Dirac states close to the chemical potential, connecting a light bulk d band to two heavy bulk f bands. Each state includes a Fermi-liquid-like quasiparticle decay rate $\propto \omega^2$ [46]. We simulated each termination by adjusting the energies of the f and d bands to match our STM spectra. Specifically, in the 1×1 spectral-function simulation, the occupied states are shifted down by 20 meV relative to the 2×1 simulation. We simulated ARPES spectra by computing an equal-weighted average of the spectral functions for each surface, then convolving the result with a Gaussian kernel that accounts for detector resolution and temperature broadening, as shown in right panels of Fig. 4(b). Specifically, we mimic the detectors in Ref. [18] with parameters $T = 12$ K, $\Delta E = 10$ meV, and $\Delta k = 0.04$ Å^{-1}, and Ref. [41] with parameters $T = 1$ K, $\Delta E = 3$ meV, and $\Delta k = 0.01$ Å^{-1}. In each case, our simulation captures the main features of the measured ARPES spectra as reproduced in Fig. 4(c): an apparent hybridization gap of approximately 20 meV and in-gap surface states with an apparent high velocity, which seem to extrapolate to a buried Dirac point [47].

IV. DISCUSSION

A complete understanding of the cleaved SmB_6 surface requires considering both electron-rich surfaces, such as the Sm 1×1 surface, and electron-deficient surfaces, such as the B-rich terminations. Importantly, our STM measurements have shown that the heavy Dirac surface states become flat only below the chemical potential [21], leading to a highly electron-hole-asymmetric band-bending scenario, as depicted in Fig. 4(d) and Fig. 5. In such a scenario, we expect that surplus electrons, as found on Sm 1×1 terminations, primarily populate the steeper (upper) part of the surface-state dispersion [see Fig. 1(b)], producing a notable downward shift of spectral features, as shown in Fig. 4(a). Conversely, a surface deficient of electrons, as expected for B-rich terminations, would depopulate the very flat (lower) part of the surface-state dispersion. Due to the dramatic difference in band slope (velocity) above and below the Fermi level, spectral features would be shifted upward by much less on a surface with missing electrons than they would be shifted downward on a surface with the same number of excess electrons. Indeed, on B_6 1×1 surfaces, STM measured a prominent peak at -6.5 meV [25], which is shifted upward by only 1.5 meV compared to the corresponding peak on

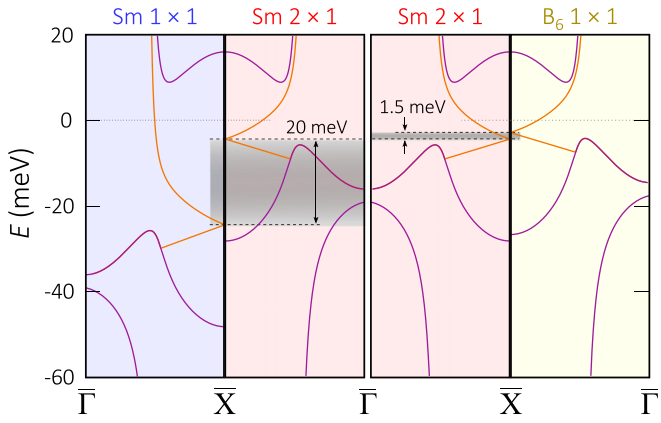

FIG. 5. Band-bending range on SmB_6 surfaces. The Sm 1 × 1 is the most negatively charged surface with a measured downward band bending of 20 meV, compared to the charge neutral Sm 2 × 1 surface. Bands on the B_6 1 × 1 surface, which is the most positively charged surface, are shifted up by 1.5 meV [25]. Therefore, our simulation including just the Sm 1 × 1 and Sm 2 × 1 surface spans more than 90% of the maximum energy range of 21.5 meV.

the neutral Sm 2 × 1 surface [see Fig. 4(a)]. Thus, the total band-bending range, defined by the most negatively charged Sm 1 × 1 termination and the most positively charged B_6 1 × 1 termination, is 21.5 meV, as shown in Fig. 5. Therefore, our ARPES simulation, using data from the two surfaces we observe, covers more than 90% of the maximum possible surface band-bending.

While our study focuses on the (001) surface, recent ARPES experiments also reported high-velocity surface states on the (110) and (111) surfaces [48,49]. These reports are surprising because both surfaces are nominally nonpolar and hence are expected to host low-velocity Dirac states. In fact, magnetothermoelectric studies have already indicated the presence of heavy metallic states on the (110) surface [50], contrary to the ARPES measurement. Under closer inspection by STM, the (110) surface appears to be inhomogeneous on small length scales [36]. The intense atomic-scale disorder may alter the local electronic environment and cause local charging, analogous to termination-dependent band bending on the (100) surface [26]. This local charging would be averaged in ARPES measurements, possibly resulting in enhanced surface-state velocities, similar to our simulations on the (100) surface [Fig. 4].

Band bending on SmB_6 may also affect the perception of the hybridization gap and explain the apparent discrepancy between its size, as reported by ARPES and STM. ARPES generally reports 15–20 meV for the part of the hybridization gap below E_F, as shown in Fig. 4(c) [14–17,25,41], while the *full* gap, as measured by STM, is only 8–15 meV [21,25–27]. In Fig. 4(b), our ARPES simulation shows a large gap below E_F, of about 25 meV, despite arising from a band structure with a gap of only 15 meV on the nonpolar surface, as measured by STM. Specifically, averaging over different surface terminations blurs the top of the bulk valence band, which introduces an apparent increase of the hybridization gap on the occupied side. The full impact of excess charge on the surface Kondo environment and d-f hybridization remains an open theoretical question [24].

V. CONCLUSION

SmB_6 is a promising platform for devices that exploit correlated topological phases, but its cubic and polar structure give rise to small, charged surface domains, on which band bending may locally distort the Dirac surface states. Using STM spectroscopy, we investigated two distinct surface terminations and measured a band shift of about 20 meV between them. These measurements guided a simulation of ARPES spectra, which captures the essential experimental features of ARPES, but remains consistent with STM conclusions [21]. Our results suggest that band bending is most pronounced on Sm-rich terminations, motivating the development of new surface treatments or epitaxial-growth techniques such as molecular beam epitaxy to achieve a more uniform termination. Control over the termination would allow the important correlated surface states to be tuned closer to the Fermi level, without introducing disorder through chemical doping, which would be advantageous for future applications [51].

All data underlying Figs. 1–5 can be accessed in Ref. [39]. The data that support the findings of this study are available from the corresponding author on reasonable request.

ACKNOWLEDGMENTS

We thank J. Denlinger, E. Rienks, and Y. Suk Eo for enlightening discussions and J. Paglione, X. Wang, Z. Fisk, and D.-J. Kim for providing the samples. Experiments were supported by National Science Foundation No. DMR-1410480 and partially as part of the Center for the Advancement of Topological Semimetals, an Energy Frontier Research Center funded by the U.S. Department of Energy (DOE), Office of Science, Basic Energy Sciences (BES) through the Ames Laboratory under its Contract No. DE-AC02-07CH11358 (STM measurements). H.P. and M.H.H. were funded by the Gordon and Betty Moore Foundation's EPiQS Initiative through Grant No. GBMF4536. C.E.M. is supported by the Swiss National Science Foundation under fellowship No. P2EZP2_175155 and P400P2_183890. J.J.P. and W.P. acknowledge Sahar Pakdel for her contribution at the initial stages of the theoretical work and financial support from Spanish MINECO through Grant No. FIS2016-80434-P, the Fundación Ramón Areces, the María de Maeztu Program for Units of Excellence in R&D (No. MDM-2014-0377), the Comunidad Autónoma de Madrid through the Nanomag COST-CM Program (No. S2018/NMT-4321), and the European Union Seventh Framework Programme under Grant Agreement No. 604391 Graphene Flagship. W.P. was funded by the CNPq Fellowship Programme (Pós-doutorado júnior) under Grant No. 405107/2017-0 and acknowledges the computer resources and assistance provided by the Centro de Computación Científica of the Universidad Autónoma de Madrid and the computer resources at MareNostrum and the technical support provided by Barcelona Supercomputing Center (FI-2019-2-0007).

[1] M. Dzero, J. Xia, V. Galitski, and P. Coleman, Topological Kondo insulators, Annu. Rev. Condens. Matter Phys. **7**, 249 (2016).

[2] P. Misra, in *Handbook of Metal Physics*, Heavy-Fermion Systems, Chapter 11 Kondo Insulators, edited by Prasanta Misra (Elsevier, 2008), Vol. 2 pp. 291–333.

[3] D. J. Kim, J. Xia, and Z. Fisk, Topological surface state in the Kondo insulator samarium hexaboride, Nat. Mater. **13**, 466 (2014).

[4] J. W. Allen, B. Batlogg, and P. Wachter, Large low-temperature Hall effect and resistivity in mixed-valent SmB_6, Phys. Rev. B **20**, 4807 (1979).

[5] J. C. Cooley, M. C. Aronson, Z. Fisk, and P. C. Canfield, SmB_6: Kondo Insulator or Exotic Metal? Phys. Rev. Lett. **74**, 1629 (1995).

[6] S. Wolgast, Ç. Kurdak, K. Sun, J. W. Allen, D.-J. Kim, and Z. Fisk, Low-temperature surface conduction in the Kondo insulator SmB_6, Phys. Rev. B **88**, 180405(R) (2013).

[7] P. Syers, D. Kim, M. S. Fuhrer, and J. Paglione, Tuning Bulk and Surface Conduction in Theproposed Topological Kondo Insulator SmB_6, Phys. Rev. Lett. **114**, 096601 (2015).

[8] M. Dzero, K. Sun, V. Galitski, and P. Coleman, Topological Kondo Insulators, Phys. Rev. Lett. **104**, 106408 (2010).

[9] F. Lu, J. Zhao, H. Weng, Z. Fang, and X. Dai, Correlated Topological Insulators with Mixed Valence, Phys. Rev. Lett. **110**, 096401 (2013).

[10] V. Alexandrov, M. Dzero, and P. Coleman, Cubic Topological Kondo Insulators, Phys. Rev. Lett. **111**, 226403 (2013).

[11] X. Chen, L. Fidkowski, and A. Vishwanath, Symmetry enforced non-Abelian topological order at the surface of a topological insulator, Phys. Rev. B **89**, 165132 (2014).

[12] D. K. Efimkin and V. Galitski, Strongly interacting Dirac liquid on the surface of a topological Kondo insulator, Phys. Rev. B **90**, 081113(R) (2014).

[13] A. Thomson and S. Sachdev, Fractionalized Fermi liquid on the surface of a topological Kondo insulator, Phys. Rev. B **93**, 125103 (2016).

[14] J. D. Denlinger, J. W. Allen, J.-S. Kang, K. Sun, B.-II Min, D.-J. Kim, and Z. Fisk, SmB_6 photoemission: Past and present, in *Proceedings of the International Conference on Strongly Correlated Electron Systems (SCES2013)*, JPS Conf. Proc. 3, 017038 (2014).

[15] N. Xu, X. Shi, P. K. Biswas, C. E. Matt, R. S. Dhaka, Y. Huang, N. C. Plumb, M. Radović, J. H. Dil, E. Pomjakushina, K. Conder, A. Amato, Z. Salman, D. McK. Paul, J. Mesot, H. Ding, and M. Shi, Surface and bulk electronic structure of the strongly correlated system SmB_6 and implications for a topological Kondo insulator, Phys. Rev. B **88**, 121102(R) (2013).

[16] N. Xu, C. E. Matt, E. Pomjakushina, X. Shi, R. S. Dhaka, N. C. Plumb, M. Radović, P. K. Biswas, D. Evtushinsky, V. Zabolotnyy, J. H. Dil, K. Conder, J. Mesot, H. Ding, and M. Shi, Exotic Kondo crossover in a wide temperature region in the topological Kondo insulator SmB_6 revealed by high-resolution ARPES, Phys. Rev. B **90**, 085148 (2014).

[17] M. Neupane, N. Alidoust, S.-Y. Xu, T. Kondo, Y. Ishida, D. J. Kim, C. Liu, I. Belopolski, Y. J. Jo, T.-R. Chang, H.-T. Jeng, T. Durakiewicz, L. Balicas, H. Lin, A. Bansil, S. Shin, Z. Fisk, and M. Z. Hasan, Surface electronic structure of the topological Kondo-insulator candidate correlated electron system SmB_6, Nat. Commun. **4**, 2991 (2013).

[18] J. Jiang, S. Li, T. Zhang, Z. Sun, F. Chen, Z. R. Ye, M. Xu, Q. Q. Ge, S. Y. Tan, X. H. Niu, M. Xia, B. P. Xie, Y. F. Li, X. H. Chen, H. H. Wen, and D. L. Feng, Observation of possible topological in-gap surface states in the Kondo insulator SmB_6 by photoemission, Nat. Commun. **4**, 3010 (2013).

[19] N. Xu, P. K. Biswas, J. H. Dil, R. S. Dhaka, G. Landolt, S. Muff, C. E. Matt, X. Shi, N. C. Plumb, M. Radović, E. Pomjakushina, K. Conder, A. Amato, S. V. Borisenko, R. Yu, H.-M. Weng, Z. Fang, X. Dai, J. Mesot, H. Ding, and M. Shi, Direct observation of the spin texture in SmB_6 as evidence of the topological Kondo insulator, Nat. Commun. **5**, 4566 (2014).

[20] S. Suga, K. Sakamoto, T. Okuda, K. Miyamoto, K. Kuroda, A. Sekiyama, J. Yamaguchi, H. Fujiwara, A. Irizawa, T. Ito, S. Kimura, T. Balashov, W. Wulfhekel, S. Yeo, F. Iga, and S. Imada, Spin-polarized angle-resolved photoelectron spectroscopy of the so-predicted Kondo topological insulator SmB_6, J. Phys. Soc. Jpn. **83**, 014705 (2013).

[21] H. Pirie, Y. Liu, A. Soumyanarayanan, P. Chen, Y. He, M. M. Yee, P. F. S. Rosa, J. D. Thompson, D.-J. Kim, Z. Fisk, X. Wang, J. Paglione, D. K. Morr, M. H. Hamidian, and J. E. Hoffman, Imaging emergent heavy Dirac fermions of a topological Kondo insulator, Nat. Phys. **16**, 52 (2020).

[22] G. Li, Z. Xiang, F. Yu, T. Asaba, B. Lawson, P. Cai, C. Tinsman, A. Berkley, S. Wolgast, Y. S. Eo, D.-J. Kim, C. Kurdak, J. W. Allen, K. Sun, X. H. Chen, Y. Y. Wang, Z. Fisk, and Lu Li, Two-dimensional Fermi surfaces in Kondo insulator SmB_6, Science **346**, 1208 (2014).

[23] B. Roy, J. D. Sau, M. Dzero, and V. Galitski, Surface theory of a family of topological Kondo insulators, Phys. Rev. B **90**, 155314 (2014).

[24] V. Alexandrov, P. Coleman, and O. Erten, Kondo Breakdown in Topological Kondo Insulators, Phys. Rev. Lett. **114**, 177202 (2015).

[25] L. Jiao, S. Rößler, D. J. Kim, L. H. Tjeng, Z. Fisk, F. Steglich, and S. Wirth, Additional energy scale in SmB_6 at low-temperature, Nat. Commun. **7**, 13762 (2016).

[26] Z. Sun, A. Maldonado, W. S. Paz, D. S. Inosov, A. P. Schnyder, J. J. Palacios, N. Yu. Shitsevalova, V. B. Filipov, and P. Wahl, Observation of a well-defined hybridization gap and in-gap states on the SmB_6(001) surface, Phys. Rev. B **97**, 235107 (2018).

[27] W. Ruan, C. Ye, M. Guo, F. Chen, X. Chen, G.-M. Zhang, and Y. Wang, Emergence of a Coherent In-Gap State in the Kondo Insulator Revealed by Scanning Tunneling Spectroscopy, Phys. Rev. Lett. **112**, 136401 (2014).

[28] S. Rößler, T.-H. Jang, D.-J. Kim, L. H. Tjeng, Z. Fisk, F. Steglich, and S. Wirth, Hybridization gap and Fano resonance in SmB_6, Proc. Natl. Acad. Sci. USA **111**, 4798 (2014).

[29] M. M. Yee, Y. He, A. Soumyanarayanan, D.-J. Kim, Z. Fisk, and J. E. Hoffman, Imaging the Kondo insulating gap on SmB_6, (2013), arXiv:1308.1085.

[30] N. Xu, H. Ding, and M. Shi, Spin- and angle-resolved photoemission on the topological Kondo insulator candidate: SmB_6, J. Phys.: Condens. Matter **28**, 363001 (2016).

[31] Y. Nakajima, P. Syers, X. Wang, R. Wang, and J. Paglione, One-dimensional edge state transport in a topological Kondo insulator, Nat. Phys. **12**, 213 (2016).

[32] D. J. Kim, S. Thomas, T. Grant, J. Botimer, Z. Fisk, and J. Xia, Surface Hall effect and nonlocal transport in SmB_6: Evidence for surface conduction, Sci. Rep. **3**, 3150 (2013).

[33] P. Giannozzi, S. Baroni, N. Bonini, M. Calandra, R. Car, C. Cavazzoni, D. Ceresoli, G. L. Chiarotti, M. Cococcioni, I. Dabo, A. Dal Corso, S. de Gironcoli, S. Fabris, G. Fratesi, R. Gebauer, U. Gerstmann, C. Gougoussis, A. Kokalj, M. Lazzeri, L. Martin-Samos *et al.*, QUANTUM ESPRESSO: A modular and open-source software project for quantum simulations of materials, J. Phys.: Condens. Matter **21**, 395502 (2009).

[34] J. P. Perdew, K. Burke, and M. Ernzerhof, Generalized Gradient Approximation Made Simple, Phys. Rev. Lett. **77**, 3865 (1996).

[35] H. J. Monkhorst and J. D. Pack, Special points for Brillouin-zone integrations, Phys. Rev. B **13**, 5188 (1976).

[36] S. Rößler, L. Jiao, D. J. Kim, S. Seiro, K. Rasim, F. Steglich, L. H. Tjeng, Z. Fisk, and S. Wirth, Surface and electronic structure of SmB_6 through scanning tunneling microscopy, Philos. Mag. **96**, 3262 (2016).

[37] L. Jiao, S. Rößler, D. Kasinathan, P. F. S. Rosa, C. Guo, H. Yuan, C.-X. Liu, Z. Fisk, F. Steglich, and S. Wirth, Magnetic and defect probes of the SmB_6 surface state, Sci. Adv. **4**, eaau4886 (2018).

[38] H. Herrmann, P. Hlawenka, K. Siemensmeyer, E. Weschke, J. Sánchez-Barriga, A. Varykhalov, N. Y. Shitsevalova, A. V. Dukhnenko, V. B. Filipov, S. Gabáni, K. Flachbart, O. Rader, M. Sterrer, and E. D. L. Rienks, A consistent view of the samarium hexaboride terminations to resolve the nature of its surface states, arXiv:1810.13380.

[39] https://doi.org/10.18126/cjyc-7ugb.

[40] S. V. Ramankutty, N. de Jong, Y. K. Huang, B. Zwartsenberg, F. Massee, T. V. Bay, M. S. Golden, and E. Frantzeskakis, Comparative study of rare earth hexaborides using high resolution angle-resolved photoemission, J. Electron Spectrosc. Relat. Phenom. **208**, 43 (2016).

[41] P. Hlawenka, K. Siemensmeyer, E. Weschke, A. Varykhalov, J. Sánchez-Barriga, N. Y. Shitsevalova, A. V. Dukhnenko, V. B. Filipov, S. Gabáni, K. Flachbart, O. Rader, and E. D. L. Rienks, Samarium hexaboride is a trivial surface conductor, Nat. Commun. **9**, 517 (2018).

[42] K. Akintola, A. Pal, M. Potma, S. R. Saha, X. F. Wang, J. Paglione, and J. E. Sonier, Quantum spin fluctuations in the bulk insulating state of pure and Fe-doped SmB_6, Phys. Rev. B **95**, 245107 (2017).

[43] Z. Zhang and J. T. Yates, Band bending in semiconductors: Chemical and physical consequences at surfaces and interfaces, Chem. Rev. **112**, 5520 (2012).

[44] J. M. Tarascon, Y. Isikawa, B. Chevalier, J. Etourneau, P. Hagenmuller, and M. Kasaya, Temperature dependence of the samarium oxidation state in SmB_6 and $Sm_{1-x}La_xB_6$, J. Phys. **41**, 1141 (1980).

[45] J. D. Denlinger, J. W. Allen, J.-S. Kang, K. Sun, J.-W. Kim, J. H. Shim, B. I. Min, Dae-Jeong Kim, and Z. Fisk, Temperature dependence of linked gap and surface state evolution in the mixed valent topological insulator SmB_6, arXiv:1312.6637.

[46] C. M. Varma, Z. Nussinov, and W. van Saarloos, Singular or non-Fermi liquids, Phys. Rep. **361**, 267 (2002).

[47] The $\Gamma_8^{(2)}$ crystal-field-split $4f$ state is missing in our STM-derived simulation, but present in ARPES experiments. The discrepancy arises because STM does not couple strongly to the $\Gamma_8^{(2)}$ state, which lacks the correct symmetry to hybridize. However, the lack of hybridization also means that the $\Gamma_8^{(2)}$ state does not play an important role in Kondo or topological physics.

[48] Y. Ohtsubo, Y. Yamashita, K. Hagiwara, S.-i. Ideta, K. Tanaka, R. Yukawa, K. Horiba, H. Kumigashira, K. Miyamoto, T. Okuda, W. Hirano, F. Iga, and S.-i. Kimura, Non-trivial surface states of samarium hexaboride at the (111) surface, Nat. Commun. **10**, 2298 (2019).

[49] J. D. Denlinger, S. Jang, G. Li, L. Chen, B. J. Lawson, T. Asaba, C. Tinsman, F. Yu, K. Sun, J. W. Allen, C. Kurdak, D.-J. Kim, Z. Fisk, and L. Li, Consistency of photoemission and quantum oscillations for surface states of SmB_6, arXiv:1601.07408.

[50] Y. Luo, H. Chen, J. Dai, Z.-A. Xu, and J. D. Thompson, Heavy surface state in a possible topological Kondo insulator: Magnetothermoelectric transport on the (011) plane of SmB_6, Phys. Rev. B **91**, 075130 (2015).

[51] J. Yong, Y. Jiang, D. Usanmaz, S. Curtarolo, X. Zhang, L. Li, X. Pan, J. Shin, I. Takeuchi, and R. L. Greene, Robust topological surface state in Kondo insulator SmB_6 thin films, Appl. Phys. Lett. **105**, 222403 (2014).